Bioorganic & Medicinal Chemistry Letters 25 (2015) 1117–1123

Contents lists available at ScienceDirect

Bioorganic & Medicinal Chemistry Letters

journal homepage: www.elsevier.com/locate/bmcl

Probing the molecular and structural elements of ligands binding to the active site versus an allosteric pocket of the human farnesyl pyrophosphate synthase

Dimitrios Gritzalis [a], Jaeok Park [b], Wei Chiu [a,†], Hyungjun Cho [a,†], Yih-Shyan Lin [a], Joris W. De Schutter [a], Cyrus M. Lacbay [a], Michal Zielinski [b,†], Albert M. Berghuis [b,c,d], Youla S. Tsantrizos [a,b,d,*]

[a] Department of Chemistry, McGill University, 801 Sherbrooke Street West, Montreal, QC H3A 0B8, Canada
[b] Department of Biochemistry, McGill University, 3655 Promenade Sir William Osler, Montreal, QC H3G 1Y6, Canada
[c] Department of Microbiology and Immunology, McGill University, 3775 Rue University, Montreal, QC H3A 2B4, Canada
[d] Groupe de Recherche Axé sur la Structure des Protéines, McGill University, 3649 Promenade Sir William Osler, Montréal, QC H3G 0B1, Canada

ARTICLE INFO

Article history:
Received 17 October 2014
Revised 26 December 2014
Accepted 29 December 2014
Available online 13 January 2015

Keywords:
Bisphosphonates
Human FPPS
Allosteric inhibitors

ABSTRACT

In order to explore the interactions of bisphosphonate ligands with the active site and an allosteric pocket of the human farnesyl pyrophosphate synthase (hFPPS), substituted indole and azabenzimidazole bisphosphonates were designed as chameleon ligands. NMR and crystallographic studies revealed that these compounds can occupy both sub-pockets of the active site cavity, as well as the allosteric pocket of hFPPS in the presence of the enzyme's Mg^{2+} ion cofactor. These results are consistent with the previously proposed hypothesis that the allosteric pocket of hFPPS, located near the active site, plays a feed-back regulatory role for this enzyme.

Bisphosphonates (BPs) are chemically stable bioisosteres of inorganic pyrophosphate that were initially developed as antiscaling, anticorrosion and water softening agents.[1,2] The subsequent discovery that BPs can also prevent bone loss in vivo opened the door to the development of therapeutic agents for the prevention of osteoclast-mediated bone diseases. The most effective of the clinically validated compounds are the nitrogen-containing BPs (N-BPs) having an aliphatic [e.g., pamidronic acid (**1a**), alendronic acid (**1b**), ibandronic acid (**1c**)] or a heterocyclic side chain, such as risedronic acid (**2**), zoledronic acid (**3**) and minodronic acid (**5**). The key biological target of N-BPs is the human farnesyl pyrophosphate synthase (hFPPS),[3] the enzyme which catalyzes the sequential condensation of isopentenyl pyrophosphate (IPP) with dimethylallyl pyrophosphate (DMAPP) to give geranyl pyrophosphate (GPP), and then catalyzes a second condensation between GPP and IPP to form farnesyl pyrophosphate (FPP). Given the strategic location of hFPPS in the mevalonate pathway, this enzyme also plays a pivotal role in controlling the intracellular levels of all human isoprenoids, as well as numerous other essential metabolites. [4]

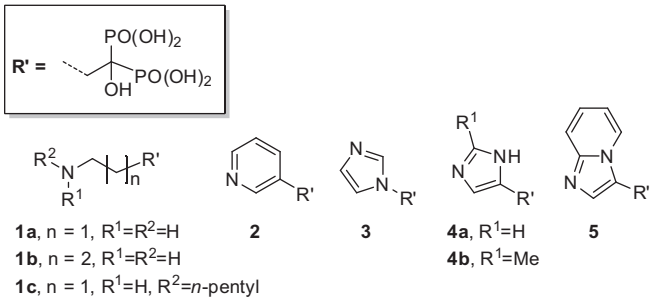

1a, n = 1, R^1=R^2=H
1b, n = 2, R^1=R^2=H
1c, n = 1, R^1=H, R^2=*n*-pentyl

2 **3** **4a**, R^1=H **4b**, R^1=Me **5**

The key pharmacophore of the current N-BP drugs is their Cα-hydroxyl bisphosphonate moiety (R′). This moiety acts as a tridentate ligand for Mg^{2+} ions in the active site of hFPPS, as well as for Ca^{2+} ions and hydroxyapatite in bone. Since removal of the Cα-hydroxyl usually leads to decreased affinity for bone, this substituent is commonly referred to as the 'bone hook'.[5] The nitrogen on the side chain of N-BPs also plays a role in the activity of these compounds. It is presumed to be protonated and participating in bifurcated hydrogen bond interactions with the side chain hydroxyl of Thr 201 and the carbonyl oxygen of Lys 200 within the hFPPS active site.[3] These interactions mimic those of the putative transition-state allylic carbocation formed during the hFPPS catalytic cycle.[6] N-BPs with an imidazole ring as part of their side chain

* Corresponding author. Tel.: +1 514 398 3638; fax: +1 514 398 3797.
E-mail address: youla.tsantrizos@mcgill.ca (Y.S. Tsantrizos).
† Undergraduate Research Participants.

http://dx.doi.org/10.1016/j.bmcl.2014.12.089
0960-894X/

(i.e., **3**, **4**, **5**) are amongst the most potent inhibitors of hFPPS, as well as the most effective therapeutics in blocking osteoclastic bone resorption. Earlier structure–activity relationship (SAR) studies at Ciba-Geigy (now Novartis) explored the direction of attachment from the imidazole to the bisphosphonate (e.g., **3** vs **4**), as well as the influence of substitution on the potency of these compounds.[7] A linker of one methylene unit between the imidazole and the Cα of the bisphosphonate, together with direct attachment of the imidazole nitrogen to the methylene linker was shown to provide optimum potency in reducing hypercalcemia (i.e., blood levels of Ca^{2+}) in rat. For example, the drug Zometa® (**3**) is approximately 4-fold more potent in vivo than analogs **4a** (i.e., EC_{50} difference reflects the dose of compound administered subcutaneously, which results in a 50% reduction of hypercalcemia in rat). Interestingly, although the methyl derivative **4b** is 50-fold less potent than **4a** and >200-fold less potent than **3**, the fused imidazole derivative **5** is nearly equipotent to **3** both in vitro and in vivo. The IC_{50} values in inhibiting hFPPS of **3** and **5** are 4.1 nM and 1.9 nM, respectively, with a minimum effective dose (MED) of 0.003 mg/kg (s.c. administration) in reducing hypercalcemia in rat.[8] A number of structurally related analogs of **5** and their corresponding azaindoles are also potent inhibitors of hFPPS.[9] Consequently, we selected the structurally related fused bicyclic imidazole (**8c**), indole (**9**) and azabenzimidazole (**10**) scaffolds for the design of compounds used in the structural investigations, described in this study.

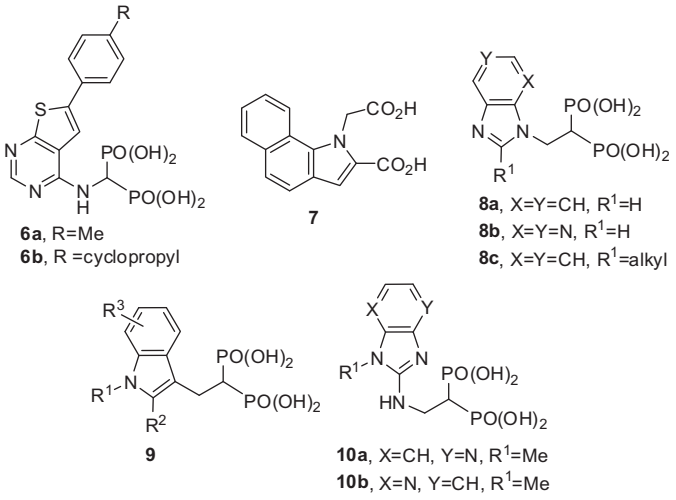

The interactions between N-BPs and their primary biological target, hFPPS, have been extensively characterized by X-ray crystallography.[3] Numerous structures of hFPPS/ligand complexes have been reported, including the binary complex of hFPPS/**2** (PDB codes: 1YQ7, 1YV5) and the ternary complex of hFPPS/**3**/IPP (PDB code: 1ZW5). These studies have revealed that in the enzyme-bound state, the bisphosphonate of N-BPs is fully ionized to the *tetra* anion and interacts with three Mg^{2+} ions. These metal-mediated interactions allow binding of N-BPs to two highly conserved aspartate-rich (DDXXD) motifs that define the allylic sub-pocket (DMAPP/GPP-binding site) of the hFPPS active site. Until very recently, all known N-BPs were found to bind exclusively in this manner and only in the allylic sub-pocket of the enzyme. In a recent report, we identified for the first time thienopyrimidine-based bisphosphonates (e.g., **6**) that exhibit a mixed binding mode.[10] We provided DSF, NMR and crystallographic data which strongly suggested that inhibitors of general structure **6** can bind mainly in the allylic sub-pocket of hFPPS in the presence of Mg^{2+} ions and in the allosteric pocket of hFPPS in the absence of Mg^{2+} ions (PDB IDs: 4JVJ vs 4LPG, respectively). The relative contributions of the two binding modes under biologically relevant conditions were estimated by ITC.[10] However, since in vitro evaluation of hFPPS activity requires Mg^{2+} as the cofactor (thus biasing the binding of bisphosphonates to the allylic sub-pocket), the ability of bisphosphonates to bind in part or exclusively in the allosteric pocket under biologically relevant conditions remained difficult to prove. In this report, we describe the design and synthesis of novel bisphosphonate inhibitors of hFPPS that are structurally related to the clinical drug **5**. We provide data which strongly suggests that some of these inhibitors can occupy simultaneously both the allylic sub-pocket and IPP sub-pocket of the active site cavity. In addition, we obtained conclusive evidence that bisphosphonates inhibitors of hFPPS can occupy the allosteric pocket of the enzyme, even in the presence of high concentrations of Mg^{2+} ions. These findings, together with the fact that bisphosphonates are structural mimics of isoprenyl metabolites (i.e., mimics of DMAPP and GPP), support the previously proposed theory that the allosteric pocket of hFPPS plays a regulatory role in product feedback inhibition.

Based on the previously reported binary and ternary structures of hFPPS/N-BP and hFPPS/N-BP/IPP complexes, it is well established that the initial occupancy of the allylic sub-pocket by an N-BP inhibitor leads to a structural change of the active site cavity from the fully 'open' to the 'half-closed' conformation.[3] This conformational transition of the protein re-defines the shape of the IPP binding sub-pocket, allowing high-affinity binding of the homoallylic substrate (IPP). Co-occupancy of the allylic sub-pocket and the IPP sub-pocket sets in motion a second conformational change, which involves folding of the C-terminal residues ^{350}KRRK^{353} over the IPP sub-pocket and complete 'closing' of the active site cavity, thus sequestering both bound ligands from bulk water. In contrast, binding of an allosteric inhibitor near the IPP sub-pocket freezes the active site cavity in the catalytically incompetent open (or half closed) conformation, even in the presence of a co-bound N-BP (PDB code: 3N46) and blocks binding of IPP; more specifically, it blocks the binding of the pyrophosphate moiety of IPP. Based on all these data, the role of the lipophilic tail of IPP in the binding contributions and the biological relevance of the allosteric pocket remained unclear.

We noted that in the enzyme bound state, the side chains of N-BP inhibitors are within van der Waals radius from the IPP hydrophobic tail (Fig. 1a–c). We also recently showed that bisphosphonate **6b** binds mainly in the allylic sub-pocket, but its pyrimidine ring protrudes into the IPP sub-pocket, thus occupying part of the region that is normally occupied by the IPP isoprenyl tail (PDB code: 4L2X; Fig. 1c). Consequently, we reasoned that N-BPs with an appropriate molecular design could possibly occupy both the allylic and IPP sub-pockets simultaneously and potentially exhibit much higher affinity for the active site cavity. Structural characterization of the interactions between such inhibitors and the enzyme could lead to the designs of novel hFPPS inhibitors with lower dependency on the bisphosphonate anchor for binding to the active site cavity.

Initially, we used an in silico model to dock benzimidazole bisphosphonates of general structure **8c** to the fully closed active site of hFPPS using GLIDE (version 5.5, Shrödinger, LLC, New York, NY 2009; standard parameters of XP-mode were used). Favourable outputs for the binding of the R^1 alkyl moiety into the IPP sub-pocket were obtained; an example of a docked molecule, where the R^1 substituent of **8c** is $-C(CH_3)$cyclopropyl, is shown in Figure 1d. However, mindful of the significant protein plasticity of hFPPS and the large conformational changes previously observed upon ligand binding to this target, we were cautious about the validity of these data.

Benzimidazole-based derivatives (e.g., **8a**,**b**) have been previously reported as potent inhibitors of hFPPS.[11] We initiated the synthesis of analogs with general structure **8c**, assuming that the R^1 alkyl group

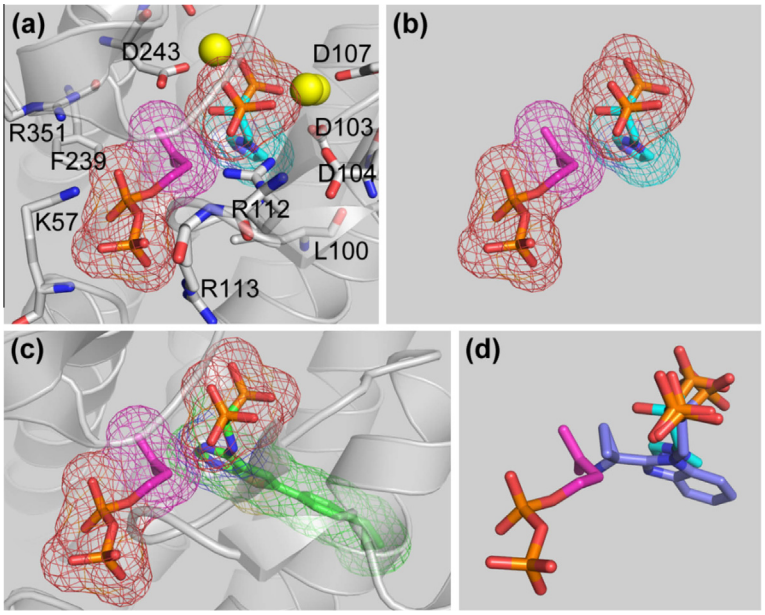

Figure 1. Ligands in the active site of hFPPS. (a) Structure of the hFPPS/**3**/IPP complex (PDB ID: 1ZW5).[3a] The surface of the ligands is represented in mesh. (b) The protein is removed to clearly show the close contact between the two ligands. (c) Superimposition of the hFPPS/**3**/IPP and hFPPS/**6b**/PPi ternary structures (PDB codes: 1ZW5 and 4L2X, respectively); **3** and PPi are omitted for clarity. The potential steric clash between the thienopyrimidine core of **6b** and the prenyl tail of IPP is evident (closest carbon-to-carbon contact is less than 2.7 Å). (d) Compound **8c** [where the R^1 is –C(CH_3)cyclopropyl] docked in the active site of the fully closed protein (PDB codes: 1ZW5) using GLIDE and superimposed with **3** and IPP; the protein was removed to clearly show the binding proximity between the R^1 alkyl moiety of **8c** and the prenyl tail of IPP. The carbon backbone of **3**, **6b**, **8c** and IPP are highlighted in cyan, green, blue and magenta, respectively. Oxygen, nitrogen, sulfur and phosphorus atoms are colored in red, blue, yellow and orange, respectively. Yellow spheres represent Mg^{2+} ions.

could mimic the prenyl tail of IPP. However, in our hands these compounds were found to be chemically unstable and further profiling in biological or structural assays were not pursued. We subsequently explored structurally related indoles **9** (Table 1). Inhibitors **9a**–**9f** were prepared via the classical Madelung indole synthesis from commercially available 2-methyl aniline (**11**). The aniline was reacted with various acid chlorides and the amide product was cyclized to the indole **12** in the presence of *n*-BuLi (Scheme 1). Alkylation of the indole nitrogen was easily achieved with alkyl halides in the presence of NaH. The indole scaffold was then reacted with tetraethyl ethene-1,1-diylbis(phosphonate) under acidic conditions to introduce the C-3 bisphosphonate side chain, which was then deprotected with TMSBr/MeOH as previously reported (Scheme 1).[12] Analogs with an aryl or heteroaryl substituent at R^3 were prepared starting with *p*-bromoaniline (**13**) via a modified Fischer indole synthesis, followed by Suzuki–Miyaura cross-coupling to obtain the key fragment **14** (Scheme 1). Reduction of the ethyl ester **14** followed by oxidation provided the aldehyde **15**, which was reacted with various Grignard reagents to give the secondary alcohol **16**. Re-oxidation of **16**–**17**, followed by a Wittig reaction provided intermediates with an olefinic branched alkyl substituent at C-2 (**18**). Hydrogenation and alkylation at the nitrogen (**19**), followed by introduction of the bisphosphonate gave analogs with a branched R^2 moiety, such as inhibitor **9i** (Scheme 1, Table 1).

Azabenzimidazoles of general structure **10** were also synthesized following the reactions shown in Scheme 2. The aminopyridines **21** and **23** were converted to the diamines **22** and **24**, respectively, with an alkyl amine (Scheme 2).[13] Carbonylation of these diamines with 1,1′-cabonyldiimidazole (CDI), provided imidazolone intermediates **25**, which were converted to the chloride **26** with $POCl_3$ as previously reported.[14] Subsequently, displacement of the chloride with ammonia (**27**), followed by coupling with tetraethyl ethene-1,1-diylbis(phosphonate) and hydrolysis of the bisphosphonate tetraesters (**28**) gave compounds **10** (e.g., **10a**,**b**; Table 1) in good overall yields.

Table 1
Indole-(**9**) and azabenzimidazole-based (**10**) inhibitors of the human FPPS; (a) structures of compounds, (b) % inhibition of hFPPS at 10 μM of inhibitors (numbers indicate the average of three independent determinations)

(a)

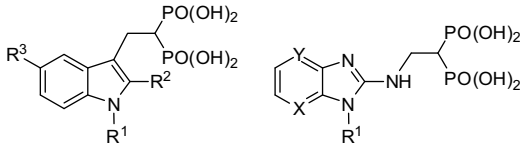

9a, R^1=Me, R^2=R^3=H
9b, R^1=Et, R^2=R^3=H
9c, R^1=*i*-Pr, R^2=R^3=H
9d, R^1=R^2=Me, R^3=H
9e, R^1=R^3=H, R^2=Me
9f, R^1=R^3=H, R^2=*t*-Bu
9g, R^1=R^3=H, R^2=CH(CH_3)CH(CH_3)$_2$
9h, R^1=R^3=H, R^2=CH(CH_3)cyclopentyl
9i, R^1=H, R^2=CH(CH_3)CH(CH_3)$_2$, R^3=Ph

10a, X=CH, Y=N, R^1=Me
10b, X=N, Y=CH, R^1=Me

(b)

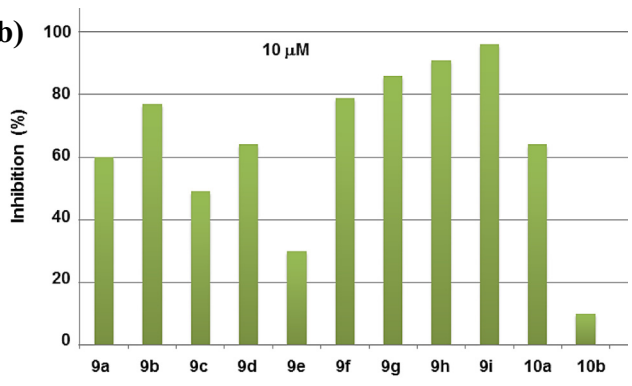

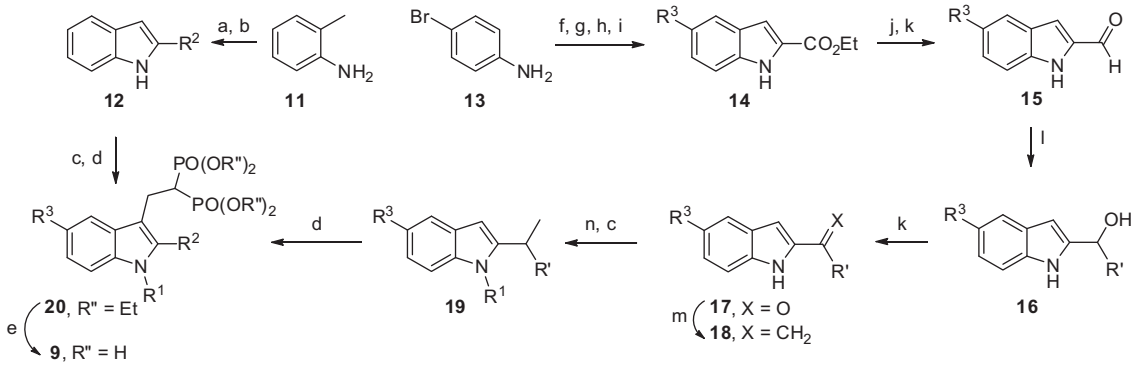

Scheme 1. Synthesis of indole-based bisphosphonates of general structure **9**. Reagents and conditions: (a) R^2COCl, CH_2Cl_2, −78 to 23 °C, 15 h, 85%; (b) *n*BuLi, THF, 0–23 °C, 90%; (c) R^1Br or R^1I, NaH, 0–23 °C, 40–90% yield; (d) tetraethyl ethene-1,1-diylbis(phosphonate), AcOH, reflux, 5d, 57%; (e) TMSBr, CH_2Cl_2, 23 °C, 5d, 98%; (f) (i) HCl, $NaNO_2$, 0 °C, 15 min, (ii) $SnCl_2$/HCl, 0 °C, 4 h, 60%; (g) ethyl pyruvate, EtOH, reflux, 15 h 85%; (h) polyphosphoric acid, 130 °C, 24 h, 45%; (i) $ArB(OH)_2$, 5% $Pd(PPh_3)_4$, K_2CO_3, dioxane/H_2O, 110 °C, 3 h, 50–70%; (j) $LiAlH_4$, THF, 0–23 °C, 15 h, 40%; (k) IBX, EtOAc, 80 °C, 3 h, 45–98%; (l) R′MgCl, THF, 0–23 °C,2 h, 80%; (m) Ph_3PMeBr, THF, 0–23 °C, 3 h, 90%; (n) H_2, Pd/C, MeOH, 23 °C, 4 h, 90%.

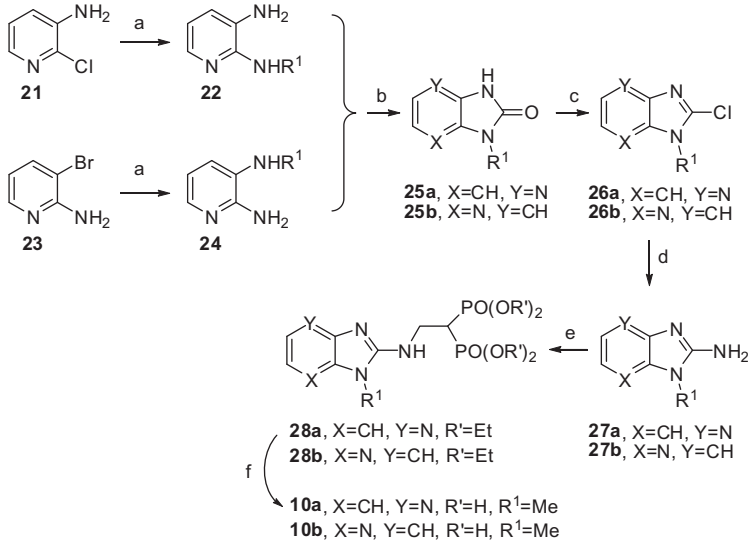

Scheme 2. Synthesis of indole-based bisphosphonates of general structure **10**. Reagents conditions: (a) R^1NH_2, $CuSO_4{\cdot}H_2O$, mw 160 °C, 1 h, 65–70%; (b) CDI, THF, 23 °C, 15 h (50–70%); (c) $POCl_3$, mw, 125 °C, 30 min (45–50%); d) 28% $NH_4OH_{(aq)}$, 100 °C, 15 h (75–80%); (e) tetraethyl ethene-1,1-diylbis(phosphonate), CH_2Cl_2/DMF, 23 °C, 15 h, (60–65%); (f) (i) TMSBr, CH_2Cl_2, (ii) MeOH (80–90%).

Representative analogs of indole (**9**) and azabenzimidazole (**10**) bisphosphonates were initially screened in our hFPPS inhibition assay at a fixed concentration of 10 μM using compound **2** and **7** as the positive controls. The inhibition data observed for some of the most important analogs are summarized in Table 1 (% inhibition of hFPPS; average values of triplicate measurements with standard deviation <10%). The main objective of this study was to probe the ability of a single bisphosphonate inhibitor to simultaneously occupy both the allylic and IPP sub-pocket of the active site cavity and also possibly bind in the allosteric pocket under biologically relevant conditions (i.e., in the presence of Mg^{2+}). Thus a detailed structure–activity relationship study was not pursued and a full dose response inhibition curve (IC_{50}) was determined only for the most potent analogs **9i** (1.1 μM); the IC_{50} values of N-BP drug **2** (11 nM) and the allosteric inhibitor **7** (0.92 μM) were also determined under the same assay conditions.

The inhibition observed with analogs **9a**,**b**,**c** suggested that small alkyl groups at R^1 (i.e., methyl, ethyl, isopropyl) did not adversely affect potency (Table 1). Similarly, a small alkyl substituent at R^2 was also well tolerated (e.g., **9d**,**e**,**f**). However, removal of the R^1 alkyl group from the indole nitrogen (Table 1; **9d** vs **9e**), resulted in some loss of potency, possibly due to the decrease in the basicity of that nitrogen (in silico docking suggested that this nitrogen could be involved in H-bonding with Thr 201 and Lys 200). Interestingly, the azabenzimidazole **10a** was found to be equivalent in potency to the indole **9a**, whereas **10b** was inactive. Although the exact mode of binding of these analogs is not yet confirmed crystallographically, binding of **10a** in the allylic sub-pocket was confirmed by competition studies using ^1H line broadening NMR. Broadening of the ^1H resonances of inhibitor **10a** were observed in the presence of Mg^{2+} ions and hFPPS (Fig. 2), suggesting fast exchange between the free and enzyme-bound state. Addition of inhibitor **2** to the same NMR sample restored the ^1H resonances of **10a**, suggesting that the two compounds compete for binding in the allylic sub-pocket of the hFPPS active site (Fig. 2). However, addition of inhibitor **7** to the hFPPS/**10a** NMR solution did not produce any change in the ^1H resonances of **10a**, suggesting that this compound binds exclusively, or predominantly, in the active site.

We subsequently investigated the indoles of general structure **9** with alkyl groups at C-2 of increasing size and steric bulk, which produced an apparent (*albeit* very modest) improvement in

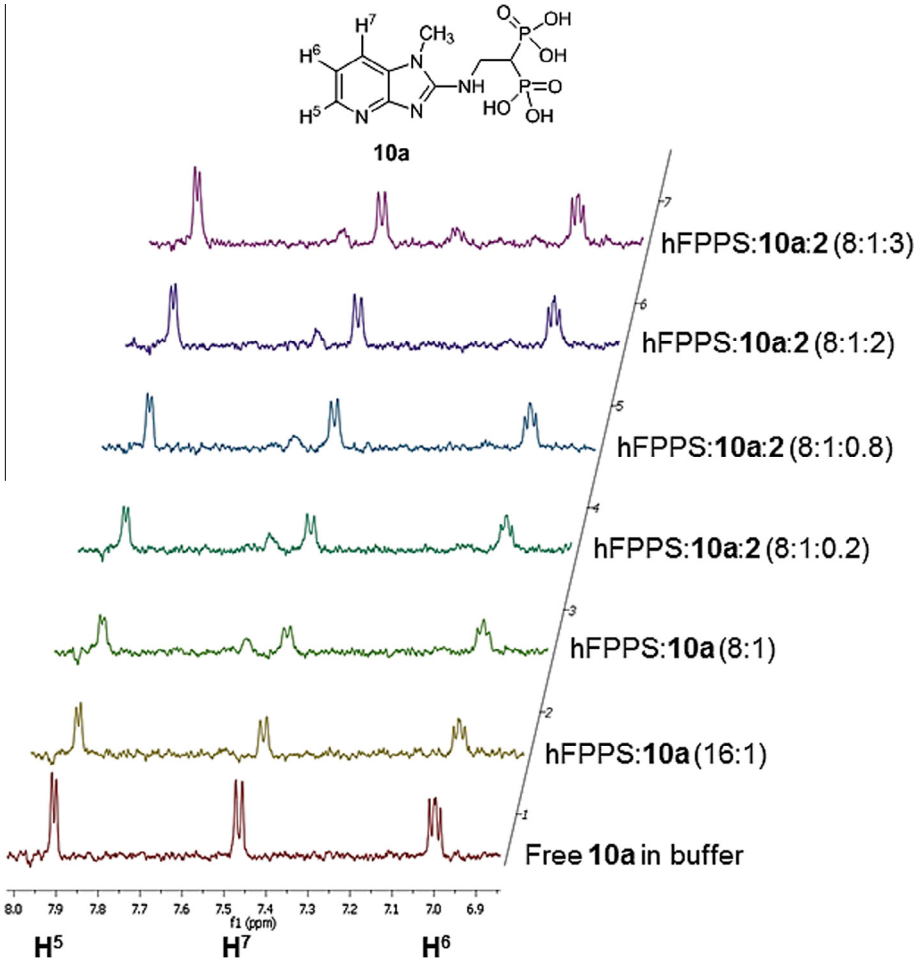

Figure 2. ^{1}H line broadening NMR studies exploring competitive binding of inhibitors **10a** and **2** in the presence of Mg^{2+} ions. Stacked spectra of inhibitor free in solution and in the presence of hFPPS and inhibitor **2**; for clarity, only a section the aromatic region is shown; the proton resonances of **10a** are labeled at the bottom of the stacked spectra. The molar ratio of ligands and protein are indicated in brackets next to each spectrum; the concentrations of **10a** and $MgCl_2$ in the sample were 100 μM and 2 mM, respectively.

potency (Table 1; **9e**–**9h**). Competitive binding of analogs **9h** and N-BP **2**, or the allosteric inhibitor **7**, was monitored by ^{1}H line broadening NMR. These studies revealed that even in the presence of excess Mg^{2+} ions, compound **9h** (i.e., the analog with the largest R^2 substituent) exhibited a dual binding mode, competing for binding mainly with **7** and to a smaller extent with the active site inhibitor **2** (Fig. 3a and b). Similarly, analog **9i**, having a smaller R^2 moiety than **9h** and more similar to the prenyl tail of IPP, exhibited clear competitive binding with both **2** and **7** in the presence of Mg^{2+} ions (Fig. 3c and d).

We characterized the binding interactions of **9i** at the allosteric pocket of hFPPS by determining the crystal structure of the hFPPS/**9i**^{allo} complex at 1.9 Å resolution (Fig. 4a). Since **9i** also competes for binding with the active site inhibitor **2** (Fig. 3c) hFPPS/**9i**^{allo} indicates specifically the binding of **9i** to the allosteric pocket. The protein is in the open conformation, and its overall structure superposes well with those of the apoenzyme (PDB code: 2F7 M) and the hFPPS/**6a**^{allo} complex (PDB code: 4LPG), with core (C_α atoms) r.m.s.d. values of 0.50 and 0.56 Å, respectively. Interestingly, however, the bound inhibitors **9i** and **6a**, as well as the protein residues within the allosteric pocket do not overlap (Fig. 4b). Similarly, the residues that form the opening of the allosteric pocket (i.e., Asn59, Arg60, Phe239, Lys347, and Ile348) show slightly different conformations in the two complexes. While the side chain of **9i** still forms π-stacking and hydrophobic interactions analogous to those observed with **6a**, its bisphosphonate moiety interacts with the protein in a significantly different manner. One of the phosphonates forms a direct polar interaction with the side chain nitrogen of Asn59 and an indirect electrostatic interaction with the guanidinium ion of Arg60 via a co-bound phosphate ion and a water molecule (Fig. 4a). Interestingly, the other phosphonate group interacts directly with the side chain carboxylate of Asp243 (Fig. 4a), presumably forming H-bonds upon protonation (inter-oxygen distances = 2.5 and 2.6 Å). Although such an interaction is highly unlikely, especially at pH ~8 (refer to SI for crystallization protocol), the electron density data provide irrefutable evidence (Fig. 4a). This interaction may represent an atypical protonation state, which has been observed previously to occur in the bound state, depending on the local environment.[15] In this light, Lys57 is of special interest as its side chain stabilizes the negative charge on the bisphosphonate moiety (together with Arg60), forming a salt bridge (Fig. 4a). As a result of this interaction, the side chain of Lys57 is fully ordered in the hFPPS/**9i**^{allo} complex, unlike in the hFPPS/**6a**^{allo} complex (Fig. 4b). Another notable difference between these two complexes is that the indole nitrogen of **9i** recruits a water molecule, which in turn forms H-bonds with the side chain oxygen of Gln242 and the main chain carbonyl of Lys347 (Fig. 4a). Although inhibitor **7** is somewhat structurally related to the indole **9i**, their binding interactions with the allosteric pocket are also clearly different (Fig. 4c). It is noteworthy that the R^2 group of **9i** does not make any close contact with the protein surface. This observation, in addition to the accumulated

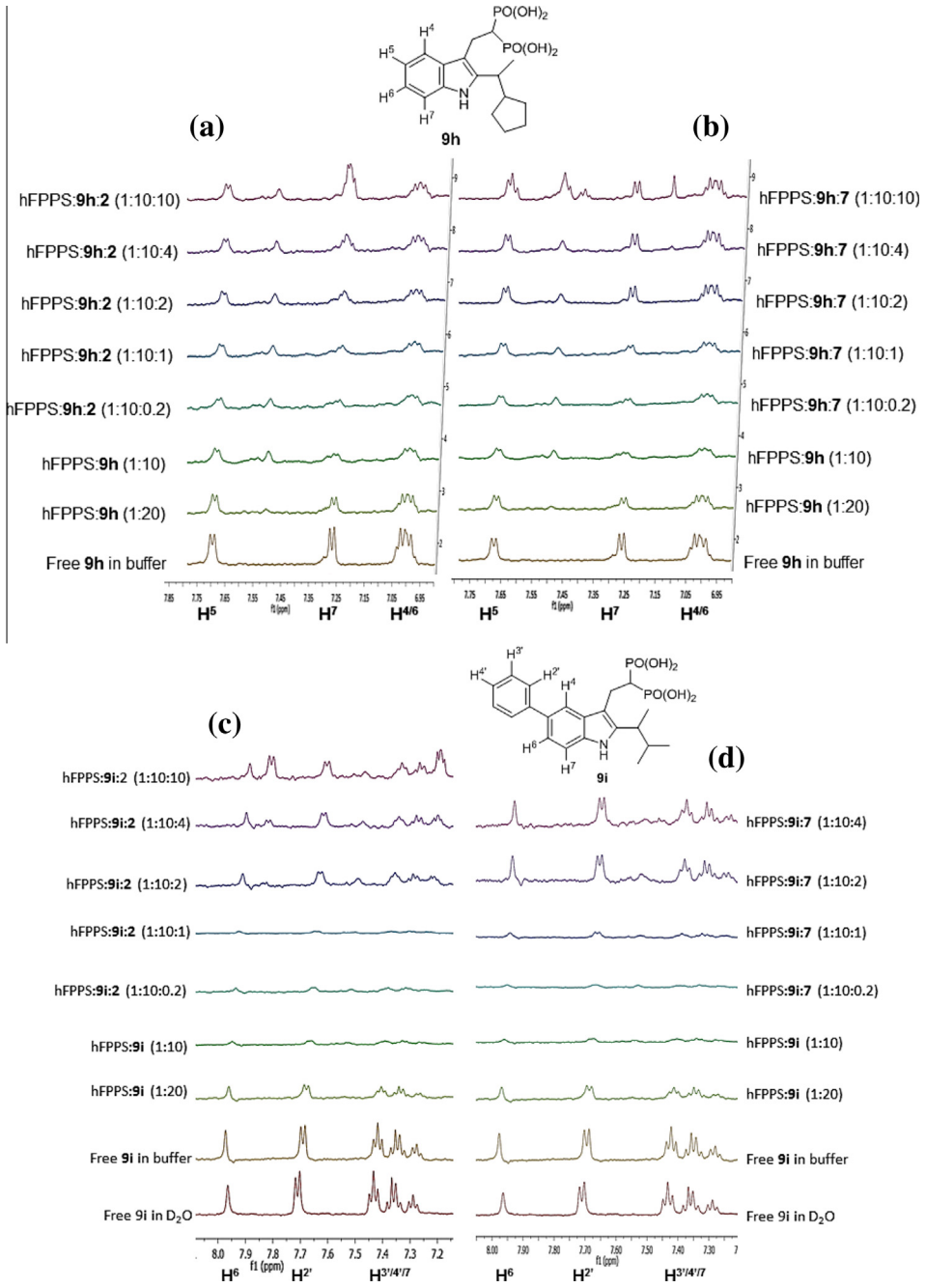

Figure 3. [1]H line broadening NMR studies exploring competitive binding of inhibitors **9h**, **9i**, **2** and **7** in the presence of 20-fold molar excess of Mg^{2+} ions (the molar ratio of ligands and protein are indicated in brackets next to each spectrum; the concentrations of **9h** and **9i** in each sample were 100 μM, whereas that of $MgCl_2$ was 2 mM). Stacked spectra of inhibitors free in solution and in the presence of hFPPS and either **2** or **7**; for clarity, only sections the aromatic regions are shown; the proton resonances of **9h** and **9i** are labeled at the bottom of the stacked spectra.

knowledge on the mode of binding of bisphosphonates in the allylic sub-pocket, suggests that the observed difference in potency between analog **9e** and **9h** is likely due to favourable binding interactions of the R^2 substituent with the IPP sub-pocket.

In summary, the human FPPS has been an important therapeutic target for skeletal diseases for many years. However, recent clinical data provide evidence that hFPPS inhibitors may also be useful for the treatment of cancer and neurodegeneration.[4] In an effort to understand the molecular recognition elements that govern the binding of ligands to the active site and/or an allosteric pocket of this enzyme near the active site, we have explored the binding mode of inhibitors **9** and **10** using NMR and X-ray crystallography. Inhibitors such as **9g**–**9i** were designed to possibly simultaneously occupy both the allylic and the IPP sub-pocket of the active site. The results of our studies suggest that this objective was accomplished and that the R^2 alkyl moiety of these compounds may be binding in the region normally occupied by the prenyl tail of IPP during catalysis. Since these analogs **9g**–**9i** are less potent in inhibiting hFPPS than the simpler N-BPs (e.g., **5**), which were used as the molecular blueprints for their design, further structural optimization is required to compensate for the induced-fit ligand binding observed with this target. Interestingly, inhibitor **9i** appears to have a higher affinity for binding in the allosteric pocket of hFPPS than the active site, confirming that

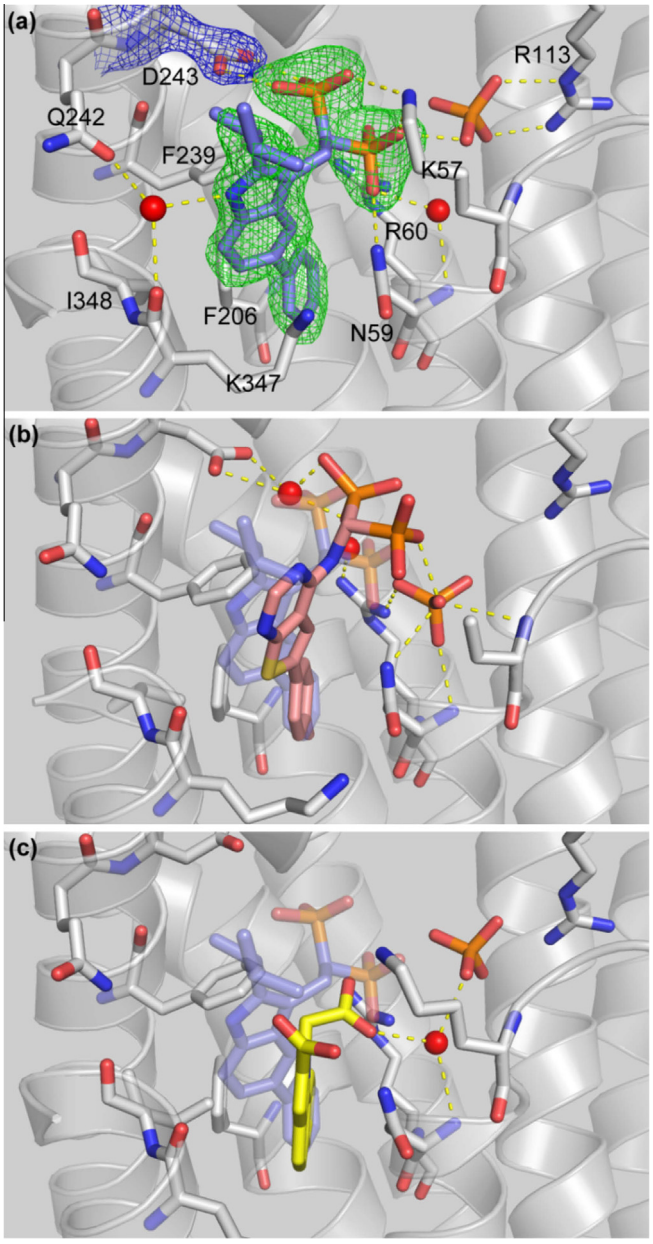

Figure 4. Bisphosphonate binding at the hFPPS allosteric site. (a) Structure of the hFPPS/**9i**^{allo} complex (PDB code: 4QXS). The green mesh represents a simulated-annealing omit map ($F_O - F_C$, contoured at 3 sigma) for **9i**, and the blue mesh, a $2F_O - F_C$ map (1 sigma) for Asp243. (b) Previously determined structure of the hFPPS/**6a**^{allo} complex (PDB code: 4LPG) shown in the same orientation. The structure of the hFPPS/**9i**^{allo} complex is superposed, with only the inhibitor displayed semitransparently. (c) The structure of the hFPPS/**7** complex (PDB code: 3N6 K) with **9i** superposed. The carbon backbone of **9i**, **6a** and **7** are highlighted in blue, pink and yellow, respectively. Oxygen, nitrogen, sulfur and phosphorus atoms are colored in red, blue, yellow and orange, respectively. Red spheres represent water molecules.

bisphosphonates can bind to this allosteric pocket under physiologically relevant conditions (i.e., in the presence of Mg^{2+} ions). These findings are consistent with the previously proposed theory that the allosteric pocket adjacent to the IPP sub-pocket plays a regulatory role in hFPPS catalysis and may be sensitive to the intracellular levels of isoprenyl pyrophosphates. Similar to the active site cavity, the structure of this allosteric pocket is flexible and can accommodate various scaffolds binding in slightly different orientations; such biological targets are not uncommon, but they make the design of high affinity ligands more challenging.

Acknowledgments

We are greatful to C.-Y. Leung for his assistance with the in vitro inhibition assays.

We gratefully acknowledge the financial support from the Natural Sciences and Engineering Research Council of Canada (NSERC) and the Canadian Institute of Health Research (CIHR) for grants to A.M.B. and Y.S.T.

Supplementary data

Supplementary data associated with this article can be found, in the online version, at http://dx.doi.org/10.1016/j.bmcl.2014.12.089.

References and notes

1. Russell, R. G. G. *Bone* **2011**, *49*, 2.
2. Ebetino, F. H.; Hogan, A.-M.; Sun, S.; Tsoumpra, M. K.; Duan, X.; Triffitt, J. T.; Kwaasi, A. A.; Dunford, J. E.; Barnett, B. L.; Oppermann, U.; Lundy, M. W.; Boyde, A.; Kashemirov, B. A.; McKenna, C. E.; Russell, R. G. *Bone* **2011**, *49*, 20.
3. (a) Rondeau, J.-M.; Bitsch, F.; Bourgier, E.; Geiser, M.; Hemmig, R.; Kroemer, M.; Lehmann, S.; Ramage, P.; Rieffel, S.; Strauss, A.; Green, J. R.; Jahnke, W. *ChemMedChem* **2006**, *1*, 267; (b) Kavanagh, K. L.; Guo, K.; Dunford, J. E.; Wu, X.; Knapp, S.; Ebetino, F. H.; Rogers, M. J.; Russell, R. G. G.; Oppermann, U. *Proc. Natl. Acad. Sci. U.S.A.* **2006**, *103*, 7829.
4. Park, J.; Matralis, A.N.; Berghuis, A.M.; Tsantrizos, Y.S. *Fron. Chem.* **2014**, article 50, http://dx.doi.org/10.3389/fchem.2014.00050.
5. Marma, M. S.; Xia, Z.; Stewart, C.; Coxon, F.; Dunford, J. E.; Baron, R.; Kashemirov, B. A.; Ebetino, F. H.; Triffitt, J. T.; Russell, G. G.; McKenna, C. E. *J. Med. Chem.* **2007**, *50*, 5967.
6. Martin, M. B.; Arnold, W.; Heath, H. T., III; Urbina, J. A.; Oldfield, E. *Biochem. Biophys. Res. Commun.* **1999**, *263*, 754.
7. Widler, L.; Jaeggi, K. A.; Glatt, M.; Müller, K.; Bachmann, R.; Bisping, M.; Born, A.-R.; Cortesi, R.; Guiglia, G.; Jeker, H.; Klein, R.; Ramseier, U.; Schmid, J.; Schreiber, G.; Seltenmeyer, Y.; Green, J. R. *J. Med. Chem.* **2002**, *45*, 3721.
8. Takeuchi, M.; Sakamoto, S.; Kawamuki, K.; Kurihara, H.; Nakahara, H.; Isomura, Y. *Chem. Pharm. Bull.* **1998**, *46*, 1703.
9. (a) Ebetino, F. H.; Mazur, A.; Lundy, M. W.; Russell, R. G. G. WO 2010/033978 A2.; (b) Ebetino, F. H.; Mazur, A.; Lundy, M. W.; Russell, R. G. G. WO 2010/033980 A2.; (c) Ebetino, F. H.; Mazur, A.; Lundy, M. W.; Russell, R. G. G. WO 2010/033981 A2.
10. De Schutter, J. W.; Park, J.; Leung, C.-Y.; Gormley, P.; Lin, Y.-S.; Hu, Z.; Berghuis, A. M.; Poirier, J.; Tsantrizos, Y. S. *J. Med. Chem.* **2014**, *57*, 5764.
11. Simoni, D.; Gebbia, N.; Invidiata, F. P.; Eleopra, M.; Marchetti, P.; Rondanin, R.; Baruchello, R.; Provera, S.; Marchioro, C.; Tolomeo, M.; Marinelli, L.; Limongelli, V.; NovellinKwaasi, A.; Dunford, J.; Buccheri, S.; Caccamo, N.; Dieli, F. *J. Med. Chem.* **2008**, *51*, 6800.
12. Lacbay, C. M.; Mancuso, J.; Lin, Y.-S.; Bennette, N.; Götte, M.; Tsantrizos, Y. S. *J. Med. Chem.* **2014**, *57*, 7435.
13. Chrisman, W.; Knize, M. G.; Tanga, M. J. *J. Heterocycl. Chem.* **2008**, *45*, 1641.
14. Ognyanov, V. I.; Balan, C.; Bannon, A. W.; Bo, Y.; Dominguez, C.; Fotsch, C.; Gore, V. K.; Klionsky, L.; Ma, V. V.; Qian, Y.-X.; Tamir, R.; Wang, X.; Xi, N.; Xu, S.; Zhu, D.; Gavva, N. R.; Treanor, J. J. S.; Norman, M. H. *J. Med. Chem.* **2006**, *49*, 3719.
15. (a) Steuber, H.; Czodrowski, P.; Sotriffer, C. A.; Klebe, G. *J. Mol. Biol.* **2007**, *373*, 1305; (b) Czodrowski, P.; Sotriffer, C. A.; Klebe, G. *J. Chem. Inf. Model.* **2007**, *47*, 1590.